

## Origin of InGaN/GaN light-emitting diode efficiency improvements using tunnel-junction-cascaded active regions

Joachim Piprek<sup>a)</sup>

NUSOD Institute LLC, P.O. Box 7204, Newark, Delaware 19714, USA

(Received 2 December 2013; accepted 23 January 2014; published online 5 February 2014)

This Letter investigates the efficiency enhancement achieved by tunnel junction insertion into the InGaN/GaN multi-quantum well (MQW) active region of blue light emitting diodes (LEDs). The peak quantum efficiency of such LED exceeds 100%, but the maximum wall-plug efficiency (WPE) hardly changes. However, due to the increased bias, the WPE peaks at much higher input power, i.e., the WPE droop is significantly delayed, and the output power is strongly enhanced. The main physical reason for this improvement lies in the non-uniform vertical carrier distribution typically observed within InGaN MQWs. © 2014 AIP Publishing LLC. [<http://dx.doi.org/10.1063/1.4864311>]

GaN-based light-emitting diodes (LEDs) are of great interest for applications in lighting, displays, biotechnology, sensing, medical instrumentation, and other areas. However, the development of GaN-based LEDs is handicapped by a significant efficiency reduction with increasing injection current density (efficiency droop).<sup>1</sup> To overcome the efficiency droop problem, the introduction of multiple tunnel junctions was recently proposed to form cascaded active regions.<sup>2</sup> Previously, GaN-based tunnel junctions were placed between different active regions to enable dual wavelength emission.<sup>3,4</sup> Other groups improved the hole injection into the active region by implementing a tunnel junction on the p-doped side of the LED.<sup>5,6</sup>

The stacking of identical multi-quantum well (MQW) active regions with tunnel junctions in between is an intriguing concept, as it allows for the repeated use of electrons and holes for photon generation with an external quantum efficiency (EQE) above 100%. Naturally, the wall-plug efficiency (WPE = output power/input power) remains below 100% since bias and input power multiply with the number  $N$  of MQW active regions. Without specification of the LED active region, the authors of Ref. 2 base their efficiency prediction on a simple analytical model in which the stacking of  $N$  identical active regions requires  $N$ -times the input power and delivers  $N$ -times the output power for a given (low) current density. The WPE vs. current characteristics are quasi identical, but the WPE vs. input power characteristics move in the direction of the power axis with increasing number,  $N$ , of stacked active regions (cf. Fig. 5(b) in Ref. 2). As a result, the maximum low-current WPE is achieved at higher power. However, this analytical model assumes an identical carrier concentration in all quantum wells, leading to the paradox that the same WPE vs. power shift could be accomplished by simply increasing the number of quantum wells without using any tunnel junction at all. In that case, instead of the bias, the injection current would increase proportional to the total number of quantum wells and deliver the same output power vs. input power characteristic as with tunnel junctions.

In order to investigate the tunnel-junction concept more thoroughly, we here employ an advanced numerical model

in combination with available measurements. Our analysis utilizes a modified version of the APSYS simulation software.<sup>7</sup> This and other numerical tools are often used in the investigation of GaN-based LEDs.<sup>8</sup> APSYS self-consistently computes the semiconductor carrier transport equations, coupled with a quantum-mechanical model for the photon emission from the InGaN quantum wells. The built-in polarization charge density at nitride material interfaces is calculated using a recently published second-order model.<sup>9</sup> Schrödinger and Poisson equations are solved iteratively in order to account for the quantum well deformation with changing device bias and the quantum-confined Stark effect. The carrier transport model considers drift and diffusion of electrons and holes, Fermi statistics, thermionic emission at hetero-interfaces, as well as band-to-band tunneling. The ionization energy of Si donors in GaN is 20 meV. For Mg acceptors in AlGaIn, the ionization energy is scaled linearly from 170 meV (GaN) to 470 meV (AlN). Further details of our LED model can be found elsewhere.<sup>10</sup>

The GaN-LED efficiency droop phenomenon currently receives tremendous attention but the physical mechanisms behind it are still disputed.<sup>11</sup> The two commonly cited explanations for the droop are Auger recombination within the MQW active region<sup>12</sup> and/or electron leakage from the MQW into the p-doped layers of the LED.<sup>13</sup> Both droop mechanisms are included in our LED model. The coefficients for Shockley-Reed-Hall (SRH) recombination ( $A = 5 \times 10^6/\text{s}$ ) and Auger recombination ( $C = 2.4 \times 10^{-30} \text{ cm}^6/\text{s}$ ) are adjusted to find agreement with measurements (see below).

For model calibration, we first simulate a conventional LED according to published design specifications.<sup>14</sup> The reference device includes a 3  $\mu\text{m}$ -thick  $5 \times 10^{18} \text{ cm}^{-3}$  n-doped GaN layer, followed by an MQW active region comprising eight 2-nm-thick  $\text{In}_{0.12}\text{Ga}_{0.88}\text{N}$  wells and nine 15-nm-thick GaN barriers. The 45-nm-thick p- $\text{Al}_{0.15}\text{Ga}_{0.85}\text{N}$  electron blocker layer (EBL) is grown on top of the MQW, covered by a p-GaN cap layer (both doped with  $12 \times 10^{18} \text{ cm}^{-3}$  Mg). Figure 1 demonstrates the good agreement between simulated LED performance (curve “8QW”) (QW—quantum well) and published measurements (dots) of the light output power vs. current density and the bias vs. current density characteristics. Fit parameters are the photon extraction

<sup>a)</sup>piprek@nusod.org

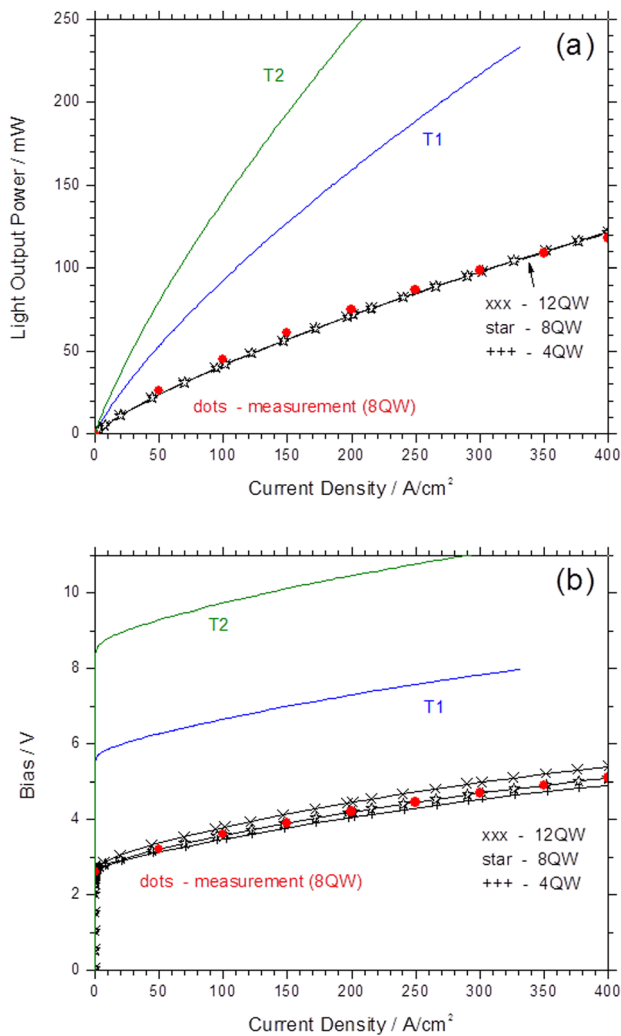


FIG. 1. Light power vs. current density (a) and bias vs. current density (b) characteristics for all five devices investigated. The device area is  $200\ \mu\text{m} \times 200\ \mu\text{m}$ , i.e., a current density of  $200\ \text{A}/\text{cm}^2$  corresponds to  $80\ \text{mA}$  total current.

efficiency of 80% and the p-contact resistivity of  $5 \times 10^{-3}\ \Omega\text{cm}^2$ , respectively. Both numbers are not reported for the reference device, and they are hard to predict theoretically. Figure 1 also plots simulated characteristics of other devices, which are explained below.

Figure 2 displays the band diagram and the radiative recombination profile near the MQW of the reference device. The eight quantum wells are strongly deformed by the built-in polarization. Only the p-side quantum wells deliver a relevant photon emission rate because of the higher carrier density in those wells. Electrons have a lower effective mass and they move more easily across the MQW than holes. Such strong MQW emission non-uniformity was also found experimentally.<sup>15</sup>

Changing the number of quantum wells from 8 to 4 or 12 does not have much effect on the characteristics in Fig. 1 (curves “4QW” and “12QW”). The bias increases slightly with thicker MQW due the small potential drop in the MQW barriers. The light output power is almost the same, which is not surprising considering the strong emission non-uniformity shown in Fig. 2. Thus, simply adding more quantum wells cannot lead to the desired LED power enhancement.

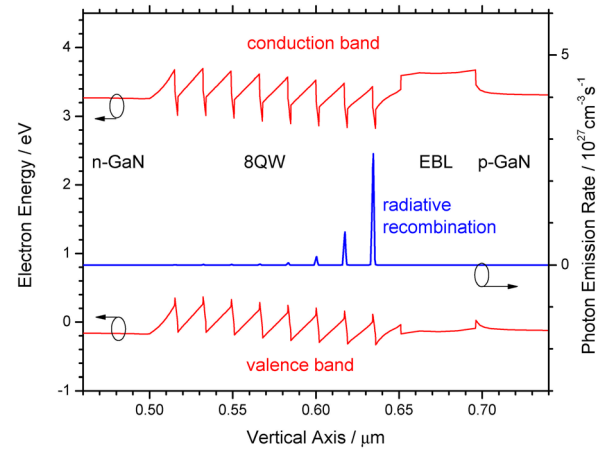


FIG. 2. Energy band diagram and photon emission rate for the reference device at  $200\ \text{A}/\text{cm}^2$  current density.

We now insert tunnel junctions into the simulated devices as illustrated in Fig. 3. The authors of Ref. 2 measured a reverse tunnel-junction resistivity as low as  $5.7 \times 10^{-4}\ \Omega\ \text{cm}^2$ , which was achieved by inserting GdN nano-islands. The corresponding tunneling process is difficult to simulate accurately, not only because of incomplete knowledge about the properties of the GdN islands but also because the tunnel probability is generally very sensitive to the actual doping profile. To still achieve a sufficiently realistic representation of the tunnel junction in our model, we assume a step-doped GaN homo-junction and adjust the effective tunneling mass in the common WKB approximation<sup>16</sup> to reproduce the measured reverse tunnel-junction resistivity for the given density of  $5 \times 10^{19}\ \text{cm}^{-3}$  donors and acceptors.

Figure 4 plots the energy band diagrams and emission profiles for the proposed tunnel-junction LEDs. The photon generation works as follows. Conduction band electrons are injected from the left-hand side, recombine within the first MQW stack, and then move inside the valence band toward the tunnel junction (holes move in the opposite direction). The tunnel junction transfers the electrons into the conduction band of the second stack, and the photon generation is then repeated in the second MQW. This process can be continued multiple times, the emission profiles of each MQW are almost identical in Fig. 4. The EBL is included in each stack to suppress electron leakage from each MQW.

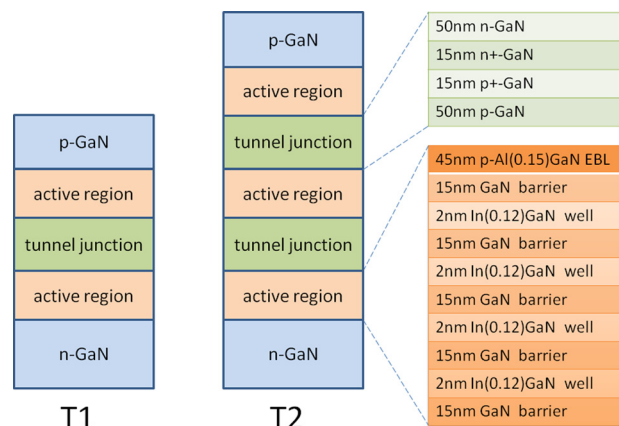


FIG. 3. Schematic structure of the two tunnel-junction LEDs proposed (T1—device with one tunnel junction, T2—device with two tunnel junctions).

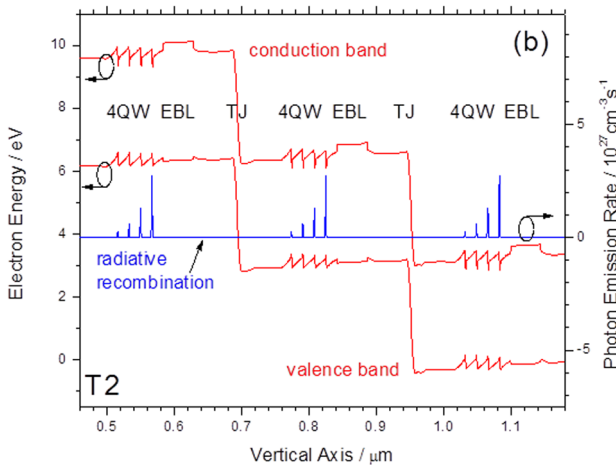
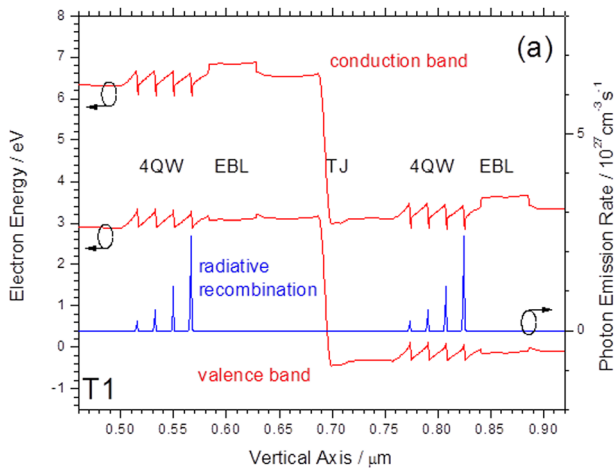


FIG. 4. Energy band diagram and photon emission rate at  $200 \text{ A/cm}^2$  current density for the two tunnel-junction LEDs shown in Fig. 3 (TJ—tunnel junction).

Figure 5 plots the external quantum efficiency (EQE) vs. current density. Without tunnel junction, the EQE characteristics for different quantum well numbers are almost identical with a peak value near 63%. The inclusion of the first tunnel junction increases this peak value to 131% and the second tunnel junction leads to a maximum external quantum

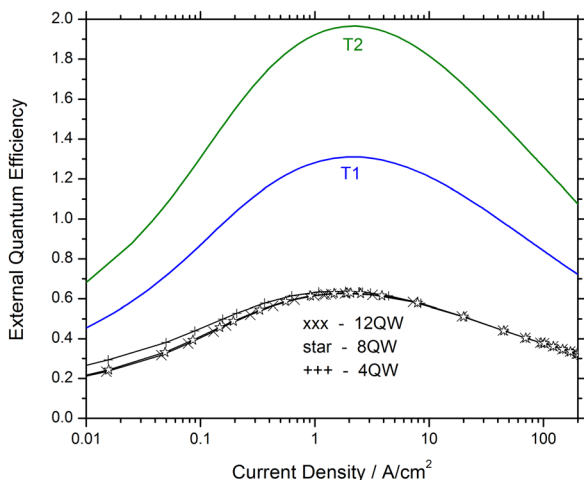


FIG. 5. External quantum efficiency vs. current density for each of the five devices simulated.

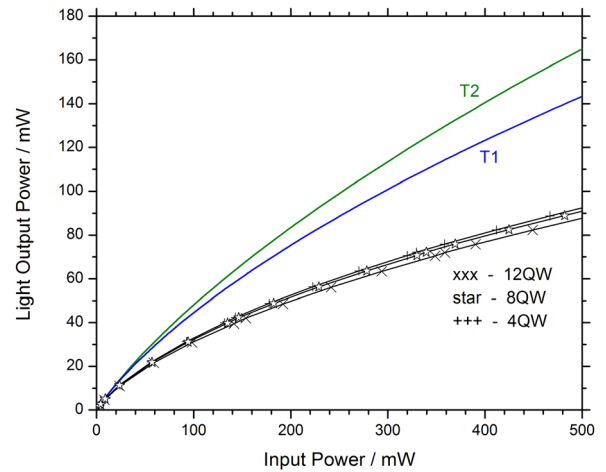


FIG. 6. Output power vs. input power for each of the five devices.

efficiency of 197%. The corresponding output power is shown in Fig. 1, which also reveals the strongly rising bias. Figure 6 shows the light output power vs. input power characteristic which gives a more instructive impression of the LED performance. For the reasons discussed above, there is not much difference between the three devices without tunnel junctions. But the introduction of a single tunnel junction raises the output power at 500 mW input power by a factor of 1.6, even if the total number of 8 quantum wells is not changed, due to the dominating role of the p-side quantum wells. Note that both cases would give identical results in the analytical model of Ref. 2. For the two cases with 12 quantum wells, the introduction of two tunnel junctions raises the light power by a factor of 1.9 at 500 mW input power. For the reference device, 500 mW input power correspond to a current density of  $245 \text{ A/cm}^2$ . The corresponding current density is  $175 \text{ A/cm}^2$  for the device with one tunnel junction and  $125 \text{ A/cm}^2$  for the device with two tunnel junctions.

Finally, Fig. 7 compares WPE vs. input power characteristics on a logarithmic scale, as shown in Ref. 2. Qualitatively similar to the results of the analytical model, the WPE peak moves towards higher power with increasing number of quantum wells, but the magnitude of the shift is larger than

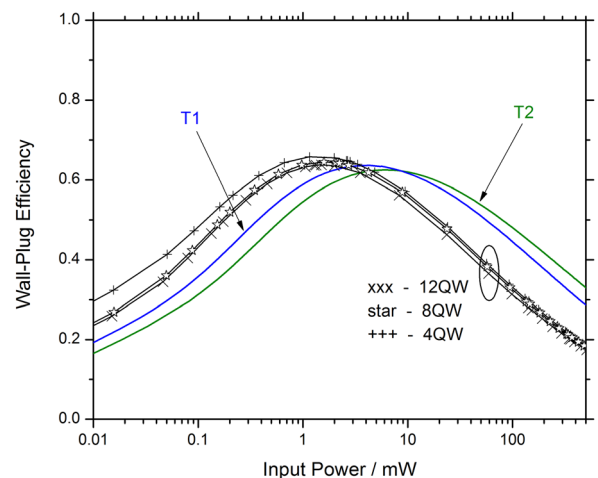


FIG. 7. Wall-plug efficiency vs. input power for each of the five devices.

predicted in Ref. 2. The single tunnel junction device (T1) shifts the WPE peak to a four times higher input power compared to the LED with 4 quantum wells without tunnel junction (4QW). Thus, much smaller numbers of tunnel junctions are needed as predicted in Ref. 2 to accomplish the desired performance improvement.

In summary, we have used self-consistent numerical LED simulation to study the performance of tunnel-junction-cascaded active regions. In contrast to a recently published analytical prediction, our simulations demonstrate that the insertion of tunnel junctions promises a significant output power enhancement compared to the same number of quantum wells without tunnel junction. The main reason for this improvement is the strongly non-uniform carrier distribution in InGaN MQW active regions. After tunnel junction insertion, the peak quantum efficiency surpasses 100% while the current density at which this peak occurs remains unchanged. However, the peak position of the wall-plug efficiency moves to higher input powers due to the increasing device bias.

<sup>1</sup>J. Piprek, *Phys. Status Solidi A* **207**, 2217–2225 (2010).

<sup>2</sup>F. Akyol, S. Krishnamoorthy, and S. Rajan, *Appl. Phys. Lett.* **103**, 081107 (2013).

- <sup>3</sup>I. Ozden, E. Makarona, A. V. Nurmikko, T. Takeuchi, and M. Krames, *Appl. Phys. Lett.* **79**, 2532–2534 (2001).
- <sup>4</sup>C. H. Chen, S. J. Chang, Y. K. Su, J. K. Sheu, J. F. Chen, C. H. Kuo, and Y. C. Lin, *IEEE Photonics Technol. Lett.* **14**, 908–910 (2002).
- <sup>5</sup>T. Takeuchi, G. Hasnain, S. Corzine, M. Hueschen, R. P. Schneider, Jr., C. Kocot, M. Blomqvist, Y.-L. Chang, D. Lefforge, M. R. Krames, L. W. Cook, and S. A. Stockman, *Jpn. J. Appl. Phys., Part 2* **40**, L861–L863 (2001).
- <sup>6</sup>S. R. Jeon, M. S. Cho, M. A. Yu, and G. M. Yang, *IEEE J. Sel. Top. Quantum Electron.* **8**, 739–743 (2002).
- <sup>7</sup>Z. M. Li, APSYS, Crosslight Software Inc., Vancouver, Canada, 2013.
- <sup>8</sup>Y.-K. Kuo, T.-H. Wang, and J.-Y. Chang, *Appl. Phys. Lett.* **100**, 031112 (2012).
- <sup>9</sup>J. Pal, G. Tse, V. Haxha, M. A. Migliorato, and S. Tomic, *Phys. Rev. B* **84**, 085211 (2011).
- <sup>10</sup>J. Piprek and S. Li, “GaN-based light-emitting diodes,” in *Optoelectronic Devices: Advanced Simulation and Analysis*, edited by J. Piprek (Springer, New York, 2005), Chap. X.
- <sup>11</sup>J. Piprek, *Proceedings of the 13th NUSOD Conference, Vancouver, Canada, 2013* (IEEE, Piscataway, 2013), pp. 107–108.
- <sup>12</sup>Y. C. Shen, G. O. Mueller, S. Watanabe, N. F. Gardner, A. Munkholm, and M. R. Krames, *Appl. Phys. Lett.* **91**(14), 141101 (2007).
- <sup>13</sup>M. H. Kim, M. F. Schubert, Q. Dai, J. K. Kim, E. F. Schubert, J. Piprek, and Y. Park, *Appl. Phys. Lett.* **91**, 183507 (2007).
- <sup>14</sup>Y. Y. Lin, R. W. Chuang, S. J. Chang, S. Li, Z. Y. Jiao, T. K. Ko, S. J. Hon, and C. H. Liu, *IEEE Photonics Technol. Lett.* **24**, 1600–1602 (2012).
- <sup>15</sup>A. David, M. Grundmann, J. F. Kaeding, N. F. Gardner, T. G. Mihopoulos, and M. R. Krames, *Appl. Phys. Lett.* **92**, 053502 (2008).
- <sup>16</sup>J. Piprek, *Semiconductor Optoelectronic Devices* (Academic Press, San Diego, 2003), p. 56.